INVESTIGATION OF THE BOUNDARY POINTS OF A SHADOW BODY OF A TRIANGLE

SCOTT EWERT

ADVISOR: DON SOLMON
OREGON STATE UNIVERSITY

ABSTRACT. Given a triangle and the directed x-rays generated by two sources, it is possible that a second convex body exists that shares the same x-rays as the triangle. This paper investigates the boundary points of the potential second convex body.

1. INTRODUCTION

Given a convex body and two sources of directed x-rays, if a convex body lies on the line connecting those two sources, then that convex body can be uniquely determined. However, if the convex body does not lie on that line, then uniqueness of the convex body is unknown. Gardner [3] conjectured that if the convex body is a polygon, then it can be uniquely determined by two sources, but if the convex body is not a polygon, then it can not be uniquely determined.

Fithian [2] investigated the case of a triangle. By placing vertices at the intersections of rays from the two sources, he showed that for all cases except one, no second convex body could exist with the same x-ray data as the triangle.

In the remaining case, if a second convex body, which will be dubbed a "shadow body" does exist, then it will have known vertices. By using these vertices and the x-ray data, additional points on the boundary of the shadow body can be found. This paper explores these additional boundary points.

2. PRELIMINARY RESULTS

Definition 2.1. *The* directed x-ray *of a set K with respect to an x-ray source p is the function* $X_pK : [0, 2\pi] \to \mathbb{R}$ *given by*

$$X_p(\phi) = X_pK(\phi) = \int_0^\infty \chi_K(t(cos(\phi), sin(\phi)) + p)dt$$

for $0 \leq \theta \leq 2\pi$*, where* χ_K *is the characteristic function of K.*

Since this paper will be dealing with convex bodies of uniform density, the directed x-ray can be interpreted as the length of intersection of the ray at angle ϕ from source p and the convex body K.

Definition 2.2. *Let the* near-side $r_p(\phi)$ *and* far-side $R_p(\phi)$ *of a directed x-ray be the first and second points of intersection, respectively, between the ray* $r = (\phi)$ *and the boundary of the convex body.*

Date: August 18, 2006.

This work was done during the Summer 2006 REU program in Mathematics at Oregon State University.

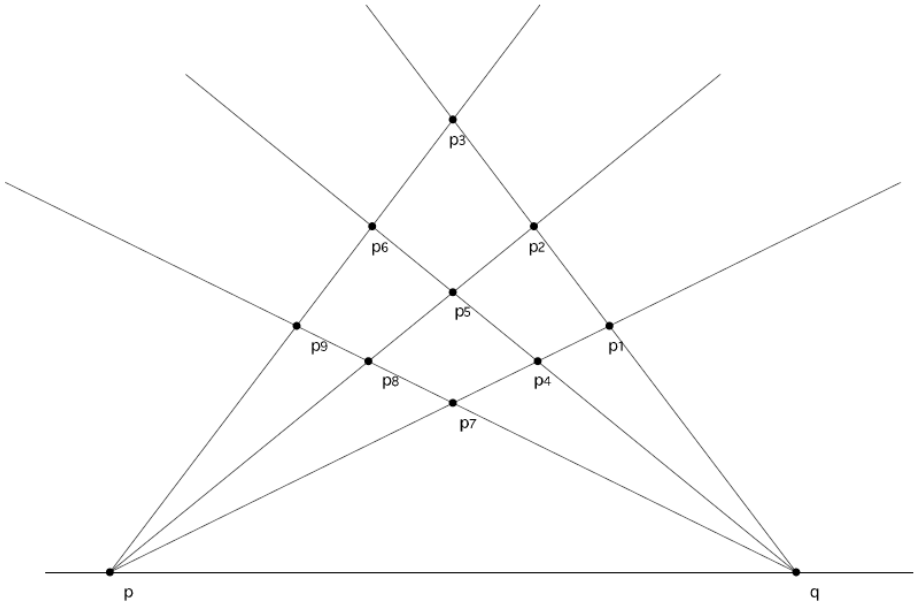

FIGURE 1. Vertex Possibilities [4]

It will be useful to extend the line segments composing the triangle and define an extension of the x-ray function to give a negative value for rays outside the triangle.

Definition 2.3. *With polar coordinates centered at p, let*

$$Y(\phi) := \textit{distance from } p \textit{ to } l_f \textit{ along ray } \phi \textit{ - distance from } p \textit{ to } l_n \textit{ along ray } \phi,$$

where l_f is the line connecting p_3 and p_4 (the extension of the far side of the triangle) and l_n is the line connecting p_4 and p_8 (the extension of the bottom side of the triangle, which is the near side near p_4) when $\phi \leq \alpha_2$, and l_n is the line connecting p_3 and p_8 when $\phi \geq \alpha 2$.

Note that $Y(\phi) = X(\phi)$ for $\alpha 1 \leq \phi \leq \alpha_3$. Also note that $Y(\phi)$ is negative for $\phi \geq \alpha_3$ and $\phi \leq \alpha_1$.

Theorem 2.4. *([4] Theorem 2.8) Let K be a convex body, p a point source, and ∂K the boundary of K. Suppose $l_p(\phi_0)$ intersects the interior of K. Then X_pK is not differentiable at $\phi = \phi_0$ if and only if at least one of the intersection points of $l_p(\phi_0)$ and ∂K is a nonsmooth point of ∂K.*

Using this theorem, it is possible to locate the vertices of a shadow body, as they must be at the intersections of rays intersecting the vertices of the triangle. Thus, it is possible to find all possible combinations of the vertices of the triangle and the vertices of the shadow body by analyzing Figure 1.

Fithian eliminated all possible combinations of triangle vertices and shadow body vertices, except for the one shown in Figure 2.

This paper will label the vertices as shown in Figure 2. In particular, the bottom vertex of the shadow body will frequently be referred to as p_7. Also note that this triangle need not be symmetric. However, for simplicity, all triangles explored further in this paper will be symmetric.

All numerical computations in this paper were done using Maple, with 80 significant digits, except for brief testing with a higher number of digits, which showed no significant deviation from

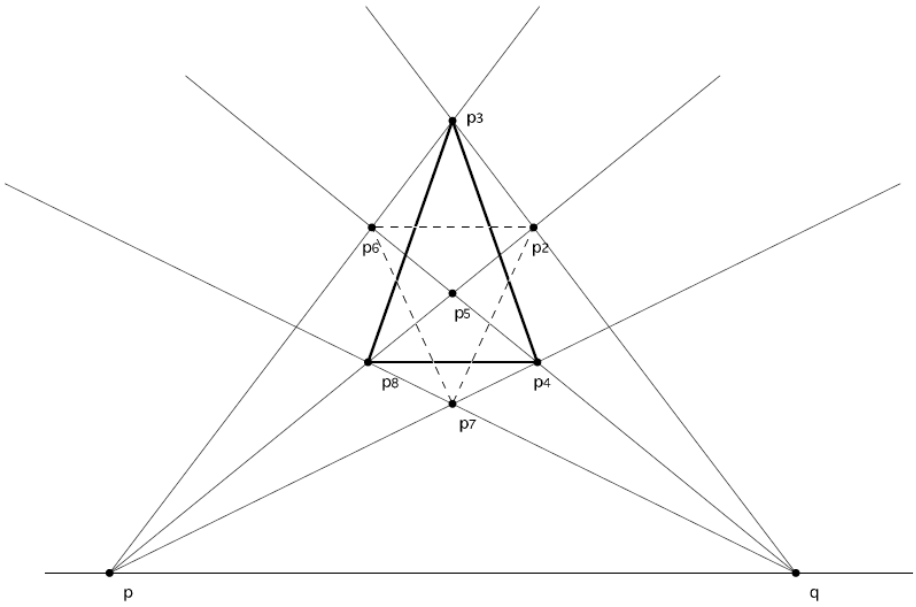

FIGURE 2. The Remaining Case [4]

results with only 80 digits (as opposed to 100 digits). Due to the length of such numbers, not all 80 digits for each number will be listed.

3. BOUNDARY POINTS

Since the vertices of the shadow body are known, by using the x-ray data, a point Γ_1[1], a boundary point on the shadow body, can be found as shown in Figure 3. From Γ_1, another point Γ_2 can be found by repeating this process. This process can be reiterated, generating a sequence Γ_j. Let Γ_0 be the point p_2.

To investigate this, a procedure was written to fix the x-ray sources, the lower two vertices of the triangle, and the x-coordinate of the top vertex p_3. Then the y-coordinate of the top vertex would be tested over a range of values, and the resulting Γ_j were examined.

This procedure uses three tests for each Γ_j, given sufficiently large j. The first two test whether or not a shadow body with these Γ_j might be convex.

Lemma 3.1. *Given $j \geq 4$, Γ_{j-4} and Γ_{j-2} of the near side of the shadow body, if the boundary point Γ_j lies below the line connecting Γ_{j-4} and Γ_{j-2}, then the shadow body can not be convex.*

Lemma 3.2. *Given $j \geq 2$, Γ_{j-2} on the near side of the shadow body, if the boundary point Γ_j lies above the line connecting Γ_{j-2} and p_7, then the shadow body can not be convex.*

These two lemmas can be proven trivially by using Figure 4. If Γ_j fails these two tests, then clearly a body with these points on its boundary can not be convex.

[1]Instead of using the notation found in Fithian and Miller's work, this paper will refer to Γ as Γ_1, and $\Gamma^{(k)}$, where k is the number of primes, will be referred to as Γ_{k+1}.

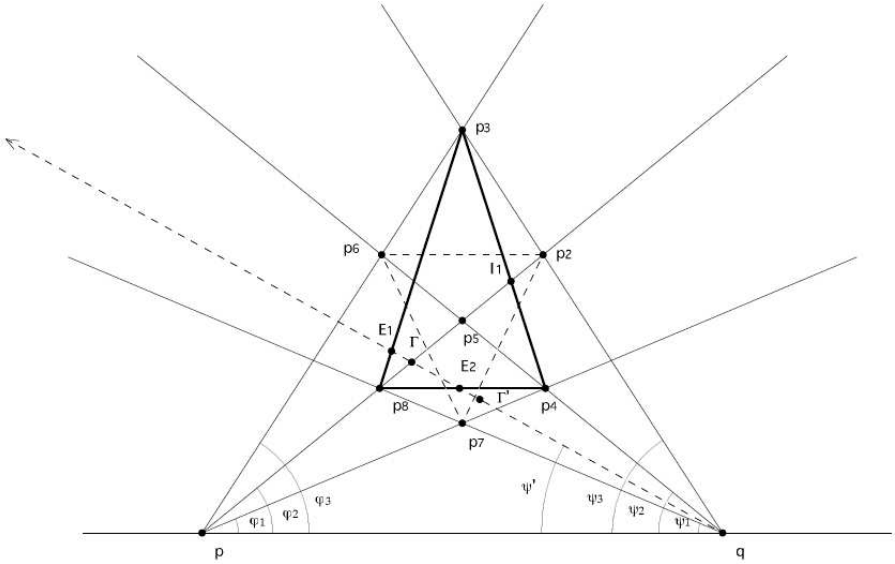

FIGURE 3. Method of Obtaining Boundary Points of the Shadow Body [4]

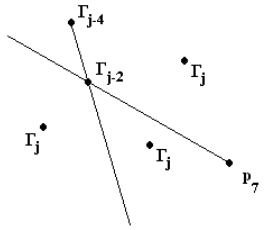

FIGURE 4. Convexity Tests

The third test checks whether or not the shadow body with these Γ_j will have the same x-ray data as the triangle. Although it is an obvious result, it is still useful.

Lemma 3.3. *If a boundary point Γ_j lies below either the line connecting source p and the bottom vertex, or the line connecting source q and the bottom vertex, then the shadow body containing Γ_j will not have the same x-ray data as the triangle.*

If Γ_j passes these three tests, then the procedure finds Γ_{j+1}, and reiterates the process.

Numerical Results As the y-coordinate of the top vertex became more precise (more digits were used), more Γ_j could be found before the convexity tests failed. This result was observed for all triangles tested.

With x-ray sources at (0,0) and (2,0), the triangle investigated most extensively had vertices at (0.5,1),(1.5,1), and (1,y), where y is the y-coordinate being varied. With $y = 6.14057$, 8 points were found before convexity failed. With $y = 6.140570022498474628037819667 80$ (30 digits), 24 points were found before convexity failed.

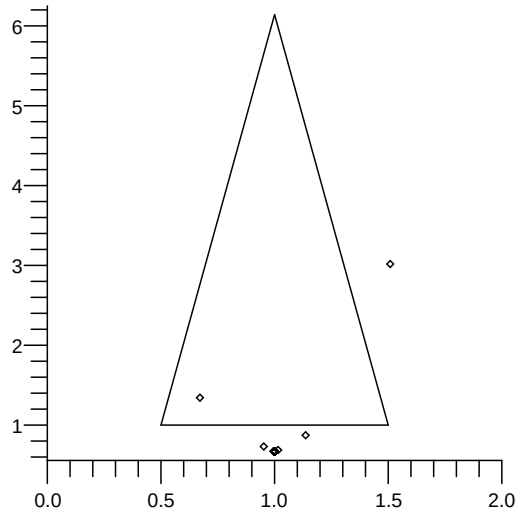

FIGURE 5. A Triangle with Γ_j Mapped for $1 \leq j \leq 50$

With $y = 6.14057002249847462803781966780232118296819440028869304965 5$ (58 digits), 36 points were found. For the rest of this paper, unless stated otherwise, the triangle referenced for calculations will be the triangle with vertices as above and this y-coordinate for the top vertex.

In all triangles tested, the Γ_j became closer to the bottom vertex as j increased. Furthermore, if the procedure were allowed to continue after convexity failed, and negative x-rays were allowed (by using $Y(\phi)$, then the Γ_j continued to approach the bottom vertex for several iterations. For example, where convexity failed at the 36nd point, Γ_{50} came the closest to the bottom vertex. Table 1 shows the distance from Γ_j to the bottom vertex p_7. Note that this point comes within $4 * 10^{-25}$ of the bottom vertex. Figure 5 shows Γ_j in relation to the triangle for $1 \leq j \leq 50$.

However, for $j > 50$, the distance between Γ_j and the bottom vertex increased as j increased. The distances as the Γ_j approached the bottom vertex seemed to follow a pattern. Similarly, the distances as the Γ_j moved away from the bottom vertex seemed to follow a pattern.

A similar result to the above occurred when only 40 digits were used in the y-coordinate of the top vertex. The next section will explore the patterns behind the Γ_j.

One final result that will be useful for the next section is to determine the tangent lines at the bottom vertex. Since the system is horizontally symmetric, let O be the point reflection point halfway between sources p and q.

Theorem 3.4. *([4] Theorem 5.1) Following Figure 6 the interior angle,* α*, of the one tangent lines at a vertex is found by solving the following equation for* α*:*

$$\frac{d(a,O)sin(2\alpha)}{cos(\phi)(cos(2\alpha)+cos(2\phi))} - X_p'(\phi) = 0$$

For the particular triangle investigated here, the equation in Theorem 3.4 has two solutions. One gives a positive interior angle α = 0.6591177145, the other a negative interior angle α = -1.239201637. These will be explored in the next section.

j	$d(\Gamma_j, p_7)$
1	0.75187021005992378512735928227
2	0.24730378668048684462327262036
3	0.08039678109420869731726676518 1
4	0.02582662873419790785014479845 3
5	0.00825577312664548388207421731 26
6	0.00263458044246425903385465060 41
⋮	
35	$1.05991422566674421445911653911 * 10^{-17}$
36	$3.37964016077021332165155521931 * 10^{-18}$
37	$1.07763131578935222742478709782 * 10^{-18}$
38	$3.43613283523382160645991516610 * 10^{-19}$
⋮	
43	$1.13257939066205755924011607350 * 10^{-21}$
44	$3.61133977136343461234752600661 * 10^{-22}$
45	$1.15151217586583391008023657143 * 10^{-22}$
46	$3.67167238487281115501969736601 * 10^{-23}$
47	$1.17086409475100350708048788354 * 10^{-23}$
48	$3.72980766894965778727475325537 * 10^{-24}$
49	$1.20101566747478429450704441616 * 10^{-24}$
50	$3.60023878893501093677851594937 * 10^{-25}$
51	$3.72038245810735444856700522864 * 10^{-25}$
52	$9.76223880189444302873183515946 * 10^{-25}$
53	$3.10237661336586624818561580900 * 10^{-24}$
54	$9.71585114046113533450046558962 * 10^{-24}$
⋮	
65	$2.80504660993156713595173620944 * 10^{-18}$
66	$8.79711645054889109029948092753 * 10^{-18}$
67	$2.75892947983513474616815879223 * 10^{-17}$
68	$8.65248506995543818386857389054 * 10^{-17}$
⋮	
96	0.00686367885486304004442771551336
97	0.02148361401624259867442394859 95
98	0.06781034238129575914294527667 11
99	0.20901542010034473800011060189 2
100	0.71138188324961183656487013850 6

TABLE 1. The Distance from Γ_j to p_7

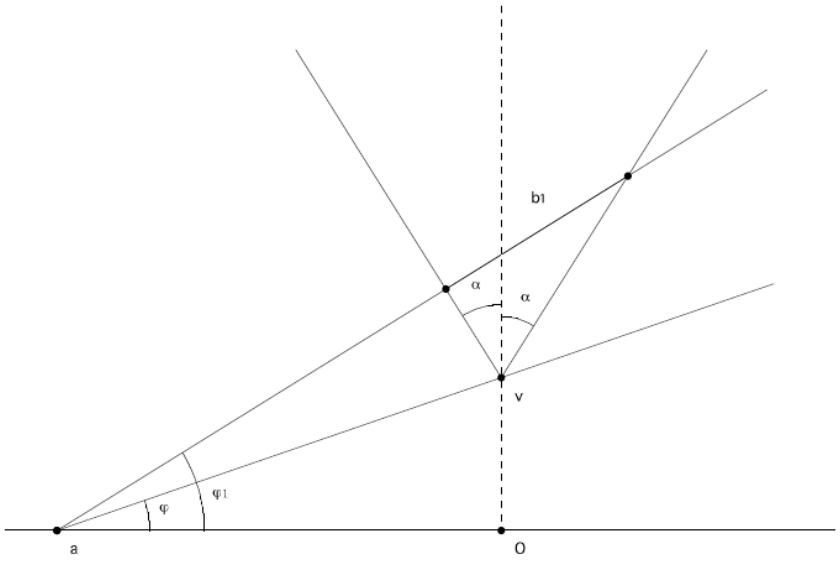

FIGURE 6. Calculation of Tangent Lines in Symmetric Case [4]

4. STABLE MANIFOLD THEOREM

Here, we attempt to analyze what is occurring near the bottom vertex by using the stable manifold theorem.

Theorem 4.1. Stable Manifold Theorem *Let $k \geq 1$, U open, $f : U \to R^2$ with v a fixed point of f. Furthermore, assume that f is C^k for $k \geq 2$. Suppose that the eigenvalues of the differential $df(v)$ are μ, λ, with $|\mu| < 1$ and $|\lambda| > 1$. Let E^s, E^u be the eigenspace corresponding to μ, λ, respectively. Then there is some neighborhood U' of v, $U' \subset U$ such that the local stable manifold for v in U',*

$$W^s(p, U', f) = \{x \, \varepsilon \, U' : \, f^j(x) \to v \text{ as } j \to \infty\}$$

is a C^k curve that is tangent to E^s (Here f^j denotes the j-fold composition of f with itself). More precisely, U' may be chosen so that in U' the stable manifold has the form

$$W^s(v, U', f) = \{v + tu_\mu + s(t)u_\lambda, -r < t < r\} \text{ where}$$

u_μ, u_λ are unit eigenvectors corresponding to the eigenvalues μ, λ respectively, and $s(t)$ is a C^k function satisfying $s(0) = s'(0) = 0$.

Now we proceed to apply this theorem. Consider the general case of a symmetric triangle. Let p, q be at $(0,0), (2a,0)$ respectively. Due to symmetry, we can define f using only one source. Let

$$F_1(r, \phi) := ((r - Y(\phi), \phi),$$

where $Y(\phi)$ is the extended x-ray function described in section 2. Here, it is clear that $F_1(p_7) = p_7$. In this case, it is advantageous to use rectangular coordinates centered at p. As such, we may write

$$F_1(x,y) := ((r - Y(\phi))cos(\phi), (r - Y(\phi))sin(\phi)).$$

Now let F_2 be the map that reflects across the vertical line through the bottom vertex p_7. Thus,

$$F_2(x,y) := (-x + 2a, y)$$

Note that this map also fixes the bottom vertex p_7, as p_7 has x-coordinate a.

Consider the composite map $f := F_2 \cdot F_1$. Then,

$$f(x,y) = ((Y(\phi) - r)cos(\phi) + 2a, (r - Y(\phi))sin(\phi)$$

It is necessary to compute $df(p_7)$. Let L be the distance from p to p_7, and let p_7 have rectangular coordinates (a,h). Let α_1 be the angle of elevation of the ray from source p through the bottom vertex of the shadow body. Since p_7 has polar coordinates (L, α_1), we have

$$cos(\alpha_1) = \frac{a}{L}, sin(\alpha_1) = \frac{h}{L}.$$

By the chain rule, we have

$$\frac{\partial f_i}{\partial x_j} = \frac{\partial f_i}{\partial r}\frac{\partial r}{\partial x_j} + \frac{\partial f_i}{\partial \phi}\frac{\partial \phi}{\partial x_j}$$

Since $r = \sqrt{x_1^2 + x_2^2}$ and $tan(\phi) = \frac{x_2}{x_1}$, we have

$$\frac{\partial r}{\partial x_1}(p_7) = \frac{a}{L} = cos(\alpha_1), \frac{\partial r}{\partial x_2}(p_7) = \frac{h}{L} = sin(\alpha_1)$$
$$\frac{\partial \phi}{x_1}(p_7) = -\frac{h}{a^2}cos^2(\alpha_1) = -\frac{sin(\alpha_1)}{L}, \frac{\partial \phi}{x_2}(p_7) = \frac{cos^2(\alpha_1)}{a} = \frac{cos(\alpha_1)}{L}.$$

Furthermore, we have

$$\frac{\partial f_1}{\partial r}(p_7) = -cos(\alpha_1), \frac{\partial f_1}{\partial \phi}(p_7) = -Y'(\alpha_1)cos(\alpha_1), \frac{\partial f_2}{\partial r}(p_7) = -sin(\alpha_1),$$
$$\frac{\partial f_2}{\partial \phi}(p_7) = -Y'(\alpha_1)sin(\alpha_1)$$

Combining these, we have

$$df(p_7) = \begin{pmatrix} -1 - \frac{Y'(\alpha_1)sin(2\alpha_1)}{2L} & \frac{Y'(\alpha_1)cos^2(2\alpha_1)}{L} \\ \frac{Y'(\alpha_1)sin^2(2\alpha_1)}{L} & 1 - \frac{Y'(\alpha_1)sin(2\alpha_1)}{2L} \end{pmatrix}$$

Note that $\det(df(p_7)) = -1$, and $\text{trace}(df(p_7)) = -\frac{Y'(\alpha_1)sin(2\alpha_1)}{L}$. Since $Y'(\alpha_1) > 0$ and $sin(2\alpha_1) > 0$, we can compute the eigenvalues and eigenvectors to be

$$\lambda = \frac{Y'(\alpha_1)sin(2\alpha_1) - \sqrt{Y'(\alpha_1)^2 sin^2(2\alpha_1) + 4L^2}}{2L} < -1$$
$$0 < \mu < \frac{Y'(\alpha_1)sin(2\alpha_1) + \sqrt{Y'(\alpha_1)^2 sin^2(2\alpha_1) + 4L^2}}{2L} < 1$$
$$\omega_\mu = (2Y'(\alpha_1)cos^2(\alpha_1), 2L + \sqrt{Y'(\alpha_1)^2 sin^2(2\alpha_1) + 4L^2}),$$
$$\omega_\lambda = (2Y'(\alpha_1)cos^2(\alpha_1), 2L - \sqrt{Y'(\alpha_1)^2 sin^2(2\alpha_1) + 4L^2}).$$

Thus, the stable manifold theorem is applicable here.

From here, the vectors at which the Γ_j approach and move away from the bottom vertex can be compared to these eigenvectors. Furthermore, if these lie on or near the stable manifold, then the distance between these points and the bottom vertex will decrease by a factor that agrees with μ to

several digits, as j increases. Similarly, if these points lie on or near the unstable manifold, then the distance between these points and will increase by a factor that agrees with λ as j increases.

Numerical Computation Again, consider the triangle with vertices at $(0.5,1)$, $(1.5,1)$, and $(1,6.14057002...)$, with the full 58 digits in the top vertex's y-coordinate. The eigenvalues are $\mu = 0.3188597793037675464$, and $\lambda = -3.1361747856173853782$. If these Γ_j lie on the stable manifold, then the ratio $d(\Gamma_{j+1}, p_7)/d(\Gamma_j, p_7)$ should approach μ as j increases. If they lie on the unstable manifold, then this ratio should approach λ.

Now consider Table 2. As shown in the table, for $1 \leq j \leq 7$, this ratio is decreasing toward μ. This pattern continues for j between 8 and 32. When j = 33, $d(\Gamma_{34}, p_7)/d(\Gamma_{33}, p_7) < \mu$. Then, for $j \geq 34$, $d(\Gamma_{j+1}, p_7)/d(\Gamma_j, p_7)$ becomes greater than μ, and begins increasing. This implies that these Γ_j could be near the stable manifold.

However, as j increases above 50, $d(\Gamma_{j+1}, p_7)/d(\Gamma_j, p_7)$ starts approaching $-\lambda$, with this ratio being closest to $-\lambda$ when j = 66. It appears that now these Γ_j may be near the unstable manifold. This could explain why these Γ_j start moving away from the bottom vertex for $j \geq 50$.

Now consider the eigenvectors: $\omega_\mu = (5.078986857, 6.556135611)$, and $\omega_\lambda = (5.078986857, -1.748733910)$. These have slopes of 1.290835317 and -.3443076266, respectively. The slope of the eigenvector corresponding to μ agrees with the slope of the tangent line with a positive interior angle computed earlier, up to more than 20 digits(up to horizontal reflection). Similarly, the other tangent line agree with the eigenvector corresponding to the unstable manifold, up to more than 20 digits (again, up to horizontal reflection).

Now consider Table 3. Table 3 shows the slope generated by the line containing Γ_j and Γ_{j+2} for even j (note that Γ_j and Γ_{j+2} will lie on the same side of the vertex). For the values of j where $d(\Gamma_{j+1}, p_7)/d(\Gamma_j, p_7)$ agrees with μ for several digits, this slope agrees with the slope of the eigenvector ω_μ for several digits as well (up to 15 digits). Similarly, for the values of j where Γ_j agrees with λ for several digits, this slope agrees with the slope of ω_λ.

This indicates that when the Γ_j are getting closer to the bottom vertex as j increases, they do so with a slope that agrees with that of the stable manifold to several digits (as many as 15, depending on j). As they start moving away from the bottom vertex, they do so at a slope that agrees with the unstable manifold to several digits (again, as many as 15, depending on j).

Figure 7 illustrates the path along which the Γ_j approach the bottom vertex. When the Γ_j approach the bottom vertex, they do so along a path near the stable manifolds. However, as the Γ_j get close to the bottom vertex, they start to veer off. As seen in Figure 8, this occurs along a path near the unstable manifold. These points must not be on the stable manifold.

A similar result occurred when the top vertex's y-coordinate was only given to about 30 digits, as well as when it was given to about 40 digits. It appears that this result will probably still occur if the top vertex is determined to any sufficiently large, finite number of digits.

It appears as though the method of perturbing the top vertex will not generate a triangle such that the Γ_j will lie on the stable manifold. Perhaps, if it could be shown that when using this method of perturbing the top vertex, the top vertex approaches some limit, then the Γ_j of the triangle with the top vertex at that limit might lie on the stable manifold. Unfortunately, at least for this class of triangles, no such limit is apparent.

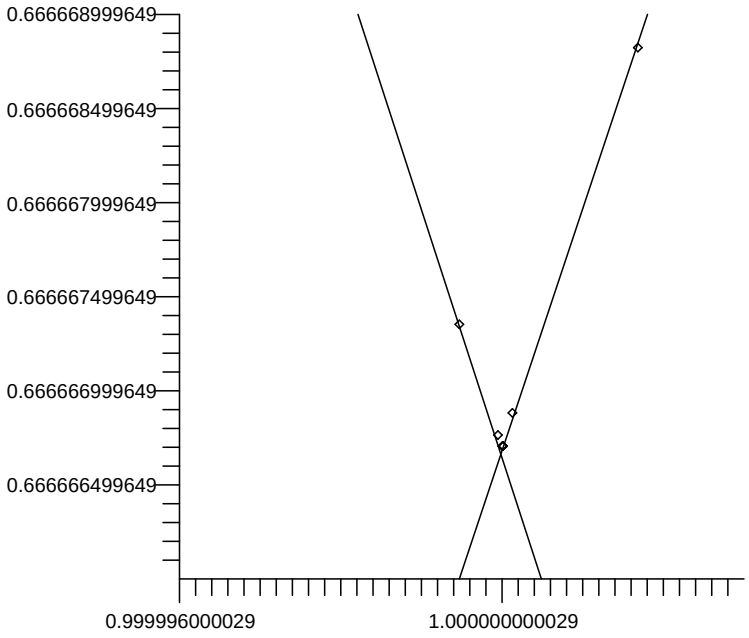

FIGURE 7. The Approach of Γ_{16} Through Γ_{20} to the Bottom Vertex, Along the Stable Manifolds

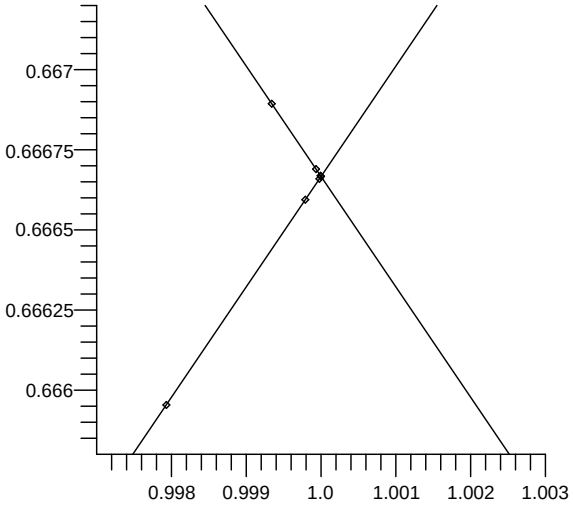

FIGURE 8. Γ_{90} Through Γ_{95} Moving Away from the Bottom Vertex, Along the Unstable Manifolds

j	$d(\Gamma_{j+1}, p_7)/d(\Gamma_j, p7)$
1	0.32891818743660135415504922772
2	0.32509320691510580729704535745
3	0.32123958674333422449237318586
4	0.31966127718844453676310441172
5	0.31911977255784298113927759540
6	0.31894313374609126235247386521
7	0.31888640383792187677484162922
⋮	
32	0.31885977930376755721231025559
33	0.31885977930376754535739388065
34	0.31885977930376759025719459518
⋮	
43	0.31886014192075384741984831519
44	0.31885621291021442817972717790
45	0.31889487230390106952302428755
46	0.31851611063444204757248076751
47	0.32238302738062827136505664303
48	0.29901833465134494609128481125
49	1.13201103407374568112582956233
50	2.68026886224759902591596843776
51	3.17375400890557452386744224860
52	3.13220670051830416516855789988
53	3.13657676677160144277129111715
54	3.13613390040583912954861567306
⋮	
65	3.13617478561738586003285111285
66	3.13617478561738535626479658144
67	3.13617478561738529601239786271
⋮	
96	3.15881480222100958583880858374
97	3.07704577599248401107008789223
98	3.44556032037360128529436038441
99	4.64180661070924982487118233065
100	0.33145637788704461007639954155

TABLE 2. The Ratio of the Distance from Γ_{j+1} to p_7 to the Distance from Γ_j to p_7

5. CONCLUSION

For triangles where the Γ_j approach the unstable manifold, it is very unlikely that a convex shadow body exists. Thus, if there exists a triangle with a convex shadow body, then it will be necessary that these Γ_j lie on the stable manifold of the bottom vertex.

j	Slope
4	1.536053760692977321799082225 77
6	1.314340689564775901719236006 37
8	1.293210941610610481828702982 23
10	1.291076704404196439421569555 61
12	1.290859857940246910325266381 42
⋮	
32	1.290835317242694752385338314 19
⋮	
64	-.344307626582654315624033057 647
66	-.344307626625240225559158182 059

TABLE 3. The Slope of the Line Containing Γ_{j+2} and Γ_j

There are several methods that may produce such a triangle. With the procedure used in this paper, the y-coordinate of the top vertex appeared to approach some limit as the number of points that passed the convexity tests increased, and the sequence of Γ_j passed closer to the bottom vertex. While the exact value of the limit is not very clear with this triangle, this is one method that could be explored.

The relation between Γ_j and Γ_{j+1} could be explored. In particular, it may be possible to find a triangle could be found such that $d(\Gamma_{j+1}, p_7)/d(\Gamma_j, p7)$ is less than 1 for sufficiently large j.

Even if a shadow body does exist for a triangle, it is still necessary to determine whether or not this shadow body is convex. The tangent lines at each Γ_j would provide insight toward whether or not the shadow body is convex. It would be useful to investigate these tangent lines.

These are all topics for future research.

REFERENCES

[1] K.J. Falconer, X-ray Problems for Point Sources. *Proc. London Math. Soc.* (3) **46** (1983), 242-262.
[2] D. Fithian, Verifying a Triangle with Two Directed X-Rays. *Undergraduate Thesis Oregon State U*. 2003
[3] R.J. Gardner, *Geometric Tomography*. Encyclopedia of Mathematics and its Applications, vol. 58. Cambridge University Press, 1995.
[4] D. Miller, Investigating Equal X-ray Bodies to the Triangle. *REU Program Oregon State U*. 2005

OREGON STATE UNIVERSITY
E-mail address: ewerts@onid.orst.edu